Mesoscale modelling of size effect on the evolution of fracture process zone in concrete

Rongxin Zhou [a, b*], Yong Lu [c], Li-Ge Wang [d, e], Han-Mei Chen [f]

[a] School of Civil Engineering, Hefei University of Technology, Hefei, China
[b] Wolfson School of Mechanical, Electrical and Manufacturing Engineering, Loughborough University, LE11 3TU, UK
[c] Institute for Infrastructure and Environment, School of Engineering, The University of Edinburgh, UK
[d] Department of Chemical and Biological Engineering, University of Sheffield, UK
[e] Process Systems Enterprise, Hammersmith, London, UK
[f] School of Architecture, University of Liverpool, L69 7ZN, UK
* Correspondence: R.Zhou2@lboro.ac.uk; rongxinzhou@hotmail.com

Abstract

A comprehensive mesoscopic investigation has been conducted to examine the evolution of the fracture process zone (FPZ), using notched plain concrete beams subjected to three-point bending as a generic representation. The concrete beams are modelled as random heterogeneous materials containing three components, namely coarse aggregates, mortar and the interface transition zone (ITZ). To better represent the fracture process in concrete, a coupled cohesive-contact interface approach is employed to model the crack initiation, crack propagation and the friction mechanisms during the fracture process. Thus, the FPZ is naturally captured in the simulation as the zone composed by microcracks along the ITZ or through the mortar matrix in the mesoscale model. The macroscopic response of load-deformation curves as well as the shapes and sizes of FPZ calculated from numerical results are validated against experimental observations and good agreement is achieved. Subsequent modelling results demonstrate that the FPZ tend to exhibit a main crack and multiple secondary microcracks. During the growth of the main crack, new microcracks initiate while some microcracks formed earlier stop growing and even close. The evolution path of the FPZ is strongly irregular due to the random spatial distribution of the aggregate particles with weak ITZs. The influence of the size effect on the FPZ is also investigated from the numerical simulation. Results show that the width of the FPZ is insensitive to the beam size but the length of the FPZ is strongly dependent on the beam size, and such characteristics of the FPZ are deemed to be intrinsic reasons for the overall size effect phenomenon in concrete structures.

Keywords: Mesoscale, concrete, micro-cracks, fracture process zone

1. Introduction

Concrete is the most widely used construction material in the world. It has a great variety of applications in the field of civil engineering. A realistic description of the failure mechanisms is very important to ensure the safety of the concrete structures [1]. However, due to the complexity of the material composition with large heterogeneities, the failure processes of concrete are still not well understood, especially under complex stress conditions. Unlike metal materials, there exists a significant localised damage zone formed by micro-cracks ahead of the crack tip when concrete fractures. This localised damage zone, which is also known as the fracture process zone (FPZ), is deemed to have a direct relationship with the macro-fracture behaviour of quasi-brittle materials including concrete and rock [2,3]. Macro-crack propagation in concrete-like materials is actually caused by the initiation, micro-crack coalescence, and the development of the FPZ [4]. As a consequence, some fundamental properties of concrete, including fracture energy and critical fracture toughness are affected by the evolution of the FPZ. Some researchers [5,6] also suggested that the FPZ ahead of a growing crack tip might be the intrinsic reason for the size dependence of the fracture parameters in concrete.

Due to the important role of the FPZ during the fracture process in concrete, various measurement techniques are already employed to track the fracture development experimentally, for example the dye penetration method [7], the scanning electron microscopy method [8], acoustic emission (AE) techniques [9], and digital image correction (DIC) method [10]. Although these experimental techniques may help depict the geometry (shape and size) of the FPZ, the composite nature of the concrete material makes it very difficult to thoroughly describe the micromechanical processes during the evolution of fracture. For this reason, various numerical models have been developed in attempt to reproduce the FPZ and thus help understand the mechanisms (e.g.[11–16]).

Modelling of concrete at mesoscale level is deemed to be a powerful means to investigate into the micromechanical processes of fracture and more broadly the failure mechanisms of composite materials under various loading conditions [17]. A mesoscale model of concrete treats the material as a composition of coarse aggregates, mortar matrix and the interface transitional zone (ITZ). There are generally three types of mesoscale concrete models in the literature, namely lattice-element (LE) model, distinct-element (DE) model and finite-element

(FE) model [18]. A key factor that determines the extent to which the mesoscopic failure mechanisms may be realistically analysed is the modelling of fractures. In the LE models [12,19], a fracture is generally represented by continuingly breaking (removing) the lattice members (beam or truss elements) when a failure criterion is met. This approach is suitable for crack opening, but it cannot accommodate possible crack closure which could happen during the complex evaluation of damage within the bulk of concrete, not to mention reversed loading. The DE or particle models possess inherent advantages in accommodating crack-induced discontinuity [20,21]. However, its ability to model the continuum and partially damaged concrete is subject to the equivalent description of the continuum properties through point contacts. Such equivalent description is difficult to generalize for different stress conditions.

Mesoscale models in a finite element framework are clearly superior in representing the nature of concrete as a non-homogeneous continuum [17,22–24] As in the general FE model of concrete, cracks may be described using either a smeared or a discrete approach. Previous research has shown some long-standing problems, such as mesh size dependency, and limited deformation modes of the standard continuum elements in the smeared crack approach when the softening behaviour is involved [18]. More recently, a continuum-damage-based mesoscale concrete model with enhancement by a nonlocal treatment is developed [14]. Thus, the evolution of the FPZ during the fracture process of notched concrete beams was successfully captured. In order to ensure a mesh independent result for both global response and local fracture process, a non-local approach with a micro characteristic length R_c was introduced into the continuum-based mesoscale concrete model. However, as it was pointed out in [14,25], the determination of the characteristic length for the mesoscale concrete model is not straightforward and can be case dependent. Moreover, there are still some inherent deficiencies of the nonlocal treatment at a mesoscale level, such as the boundary problem, the time-consuming calculation process and the 'blurred' damage process in terms of the initiation and propagation of the FPZ. All of these tend to render the non-local approach to be of a limited purpose. Moreover, a non-local based approach performs poorly in dynamic loading condition where stress wave effect is involved. To tackle these problems, a variety of techniques have been developed for regularization and tracking of cracks; however, no universal method is in sight yet for solving a general fracture problem for concrete-like materials.

Recognising the above-mentioned issues in modelling fracture using a continuum-damage-based technique, Zhou and Lu [24] developed a robust cohesive plus friction fracture model within a mesoscale finite element modelling framework to enable explicit tracking of the initiation and propagation of multiple cracks. The potential cracks in this approach are introduced via zero-thickness interface elements equipped with a fracture based constitutive law, which may be inserted along all the grid lines of the mesh. These interface lines can branch, coalesce, and eventually form new free surfaces. Understandingly, because of the high heterogeneity of concrete composites, the local stress field within the FPZ is usually subjected to the mixed-mode I-II stress conditions instead of pure mode I or pure mode II loading even under ideal extern load [26]. In the case of mixed-mode fracture, the evolution of micro-cracks within the FPZ is affected by the combination of the tensile and shear stress conditions. The shear response of micro-cracks often involves the sliding and friction mechanisms between the cracking surfaces. By allowing decohesion and friction in the ITZ between aggregate and mortar phase in the model, the above pertinent fracture characteristics can be explicitly reproduced. The model has shown its advantage in modelling the micro-crack initiation and macro-crack propagation during the fracture process in concrete-like materials under various complex loading conditions. Considering the fact that microcracks also occur within the mortar matrix [27] under quasi-static loading cases, in the present study this model is further enhanced by extending the cohesive plus friction description into the mortar phase. Thus, multi-fracture mechanisms in concrete can be explicitly simulated under general loading conditions.

This paper presents the enhanced cohesive plus friction fracture model in a mesoscale modelling framework, and the subsequent numerical investigations into local fracture processes by numerically tracking the evolution of the FPZ for concrete structures. Three-point bending beams under quasi-static loading with different sizes and geometries are simulated using a mesoscale model, in which concrete is modelled as a random heterogeneous three-phase material consisting of coarse aggregate, mortar matrix and the weaker interfacial transition zone (ITZ). The macroscopic response of the stress-strain curves, as well as the shapes and sizes of FPZ obtained from the numerical simulation are verified against experimental observations. The influences of the local stress field, friction, and the specimen size on the evolution of FPZ are identified and discussed in accordance with the numerical simulation results.

2. Numerical modelling approach

2.1 Meso-structure generation

Several studies on the generation of random meso-structure in a concrete specimen can be found in the existing literature [17,22–24,28–30] both in 2D and 3D. Previous studies [13,14,16] have indicated that as far as attention is mainly focused on the evolution of FPZ, a 2D mesoscale concrete model can be sufficient. Therefore, in this paper, a 2D mesoscale model is employed for the investigation on the fracture process of concrete using a cohesion plus contact interface approach.

The mesoscale structure of concrete is represented by a stochastic distribution of aggregates embedded in the mortar matrix. The aggregates are modelled by random polygon particles, and the nominal size of the individual aggregates obeys a given grading curve. The generation of the mesoscale geometry follows a commonly adopted take-and-place procedure [31], satisfying non-overlapping and minimum gap requirements. The procedure is programmed using Matlab. The density of the aggregates can be controlled by specifying a volume ratio. The detail procedure and steps for developing such a 2D mesoscale concrete model can be found in [31].

After generation of the mesoscopic geometric structure, ANSYS pre-processor is used to perform the FE-meshing. Triangular elements are used for better tracking the crack propagation path according to [32]. At this stage, only two components, i.e. aggregate and mortar are created. Figure 1 shows example meshed elements for aggregate and mortar components.

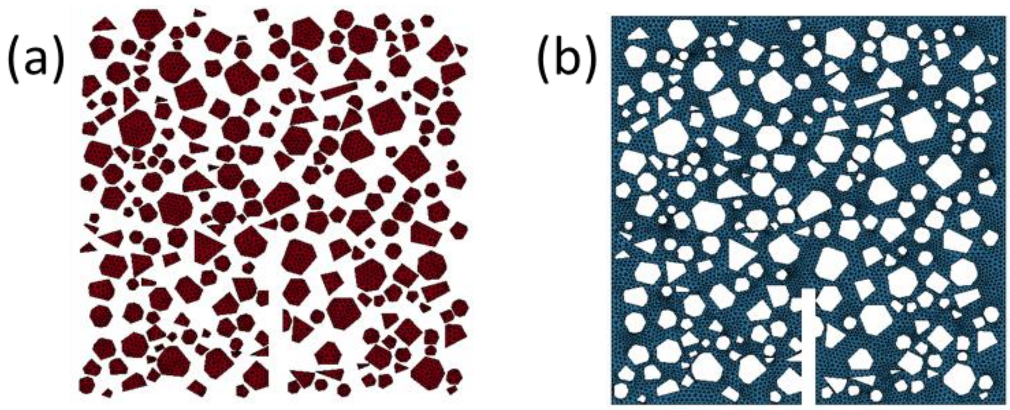

Figure 1 Representative meso-structure of concrete: (a) aggregate elements; (b) mortar elements

2.2 Inserting interface element in a mesoscale framework

After the meso-structure of the concrete has been meshed, cohesive elements are inserted along each mesh line in the meso-structure using an in-house developed code. The general steps and algorithm for inserting cohesive elements in such a meso-structure can be found in [32]. For normal concrete under quasi-static loading cases, cracks usually initiate in ITZ but can propagate through mortar matrix, especially in more advanced cracking states. Incorporating cohesive elements in the mortar matrix allows the model to fully capture the development of cracks not only at the early stage but also in more advanced states. Two groups of interface elements, namely the mortar-mortar (intra-mortar) interface elements and the aggregate-mortar interface elements, as shown in Figure 2, are identified in the present study according to the meso-structure of the concrete. An in-house MATLAB code is developed for the above-mentioned identification and cohesive element insertion. The model in the present study is an extension from [24] in which the cohesion plus friction model is employed for ITZ only. The improvements of this development from the previous model include 1) enhanced capability of simulating the crack propagation in concrete in general, 2) added capability of modelling coalescence of microcracks and the advanced cracking states. These enhancements make it possible that the full evolution process of the FPZ can then be captured, which will be discussed in detail in Section 3.

However, the aggregates in normal concrete are much stronger than the mortar matirx and the ITZ , thus no damage (or cracking) occurs within the strong aggregates under a quasi-static loading, as observed from the simulations and experimental observations [33,34] presented in the preceding studies. Therefore, in the present study, only linear-elastic material model is assumed for strong aggregates with Young's modulus around 70 GPa and no cohesive element is inserted within this component.

It is worth noting that by extending the use of cohesion plus friction interface elements into the mortar matrix, the total number of nodes and elements are increased by 9612 and 6403 (from the original 9240 and 4430 without cohesive elements in the mortar matrix), respectively for a small specimen (D = 40 mm) using a mesh grid of 1 mm. The simulation time is increased by 30% from the model in which cracking is only in the interfacial transition zone (ITZ).

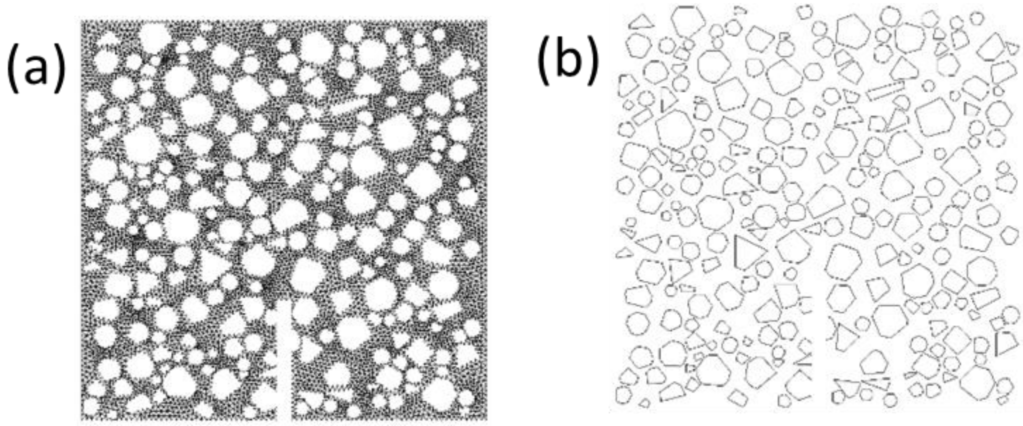

Figure 2 Coheisve elements in the meso-structure: (a) Mortar-mortar interface element; (b) Aggregate-mortar interface element

2.3 Constitutive model for the cohesive elements

As the present model permits natural initiation and growth of cracks in any path along element-to-element interfaces, it is possible to represent the cracking process and general softening behaviour of concrete via a constitutive relation between traction and opening displacement in the cohesive elements, while the bulk material outside the cohesive zone remains undamaged and in a linearly elastic state. Thus, a simple linear elastic material model is used for the brick elements, whereas a nonlinear cohesive constitutive model is attributed to the zero-thickness interface elements.

According to previous studies [24,32], a simple bilinear cohesive constitutive material model is capable of describing the failure behaviour of concrete in tension and shear dominated stress conditions. Such a cohesive model considers the irreversible damage and allows for independent definitions of the constitutive relations for different fracture modes of tension and shear (see Figure 3(a)). The model can also simulate the complex fracture behaviour by combining normal and shear traction components together. The detailed information about the constitutive description of this model and the coupling law can be found in [1]. The model requires only a few key parameters to be specified, and these include the stiffness K_N and K_S, the peak tractions, σ_I^P, σ_{II}^P and the fracture energies G_{IC}, G_{IIC} in the normal and shear directions respectively.

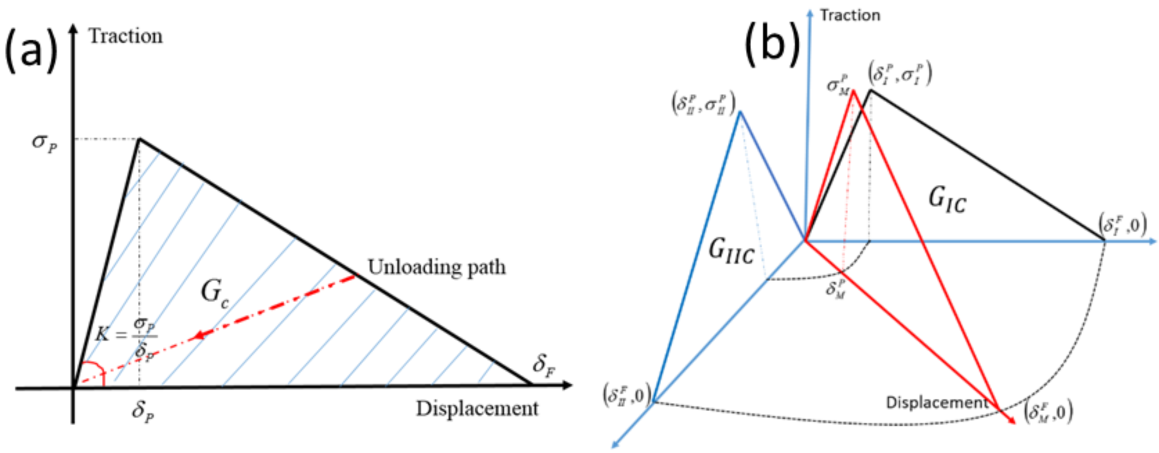

Figure 3 Cohesive constitutive model [24]: (a) in a single mode; (b) in a mixed mode

2.4 Incorporation of contact-friction mechanism

Failure of concrete materials involves the opening of the microcracks and also the frictional contact between rough surfaces. During a microcracking process, the cohesion becomes increasingly weaker while the frictional contact effect plays a more important role in influencing the residual strength. Therefore, a cohesion plus contact-friction model is deemed suitable to represent the above mechanisms in a comprehensive manner.

Generally speaking, three distinctive methods available in a general-purpose FE software such as LS-DYNA may be considered to incorporate a contact-friction algorithm, namely the kinematic constraint method, the penalty method, and the distributed parameter method. The major advantage of the penalty algorithm is that it can show very stable results without special treatment of intersecting interfaces and it does not require solving a nonlinear system of equations in every time step [35]. For this reason, the penalty method is adopted in the present study.

In a penalty-based contact algorithm, an elastic, compression-only spring is placed in the normal direction to resist penetration, as illustrated in Figure 4(a). Each slave node is checked for penetration through the master surface. If there is no penetration nothing is done but when it does penetrate, an interface force is applied between the slave node and its contact point. The magnitude of this force depends on the amount of penetration with a linear relationship. The coefficient can be regarded as the interface spring stiffness. In the tangential direction, nonlinear interface springs are used to model the friction effects between each two contact surfaces (see Figure 4(a)). According to the Coulomb Friction law, both static and kinetic frictions are considered (see Figure 4(b)). The whole process is subdivided into three stages, which can be identified from a representative numerical result from the combined model. In stage I there is almost no damage to the cohesive element. The cohesion dominates and the friction is negligible during this stage. The stage 2 is defined from the onset of fracture to the full de-cohesion. During this process, the friction and the remaining cohesion act on the same interface simultaneously. It should be noted that the frictional movement during this stage is not an explicit interface slide but constrained by the constitutive cohesion law that relates the friction force to the shear deformation, and therefore is effectively a static friction. The pure “sliding” friction stage is defined as stage 3. In this stage, the interface is fully separated thus the two contacting surfaces slide against each other with a frictional law. The friction at this stage is kinetic.

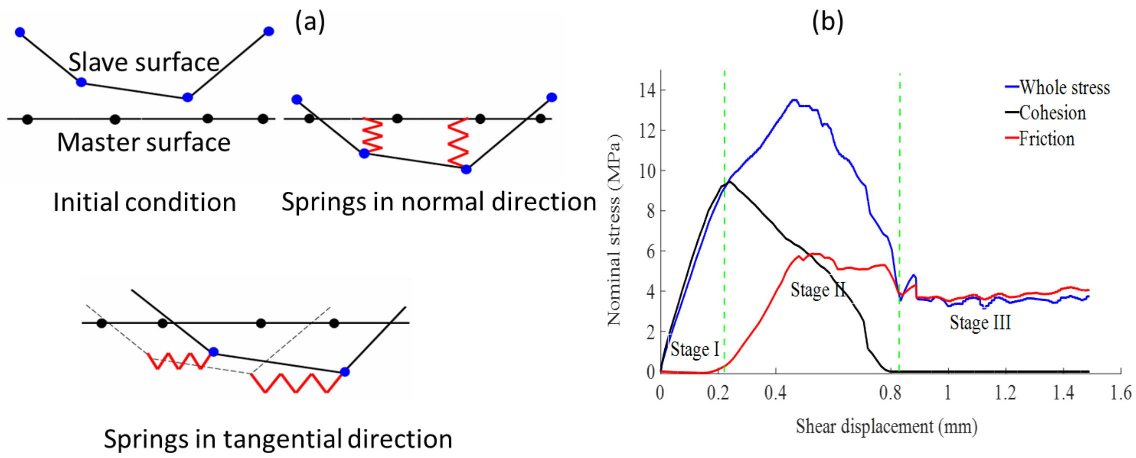

Figure 4 Combined cohesion and friction interface model: (a) sketch of the normal force and the tangential force; (b) evolution of whole shear stress combining the cohesion and friction stress.

2.5 Overview of parameters setting in the combined model

One important issue in using cohesive element is that suitable values of initial stiffness should be chosen for a subsequent comprehensive study. It is generally recognised that the initial stiffness of cohesive element, K depends on the element size, h_{mesh} and the Young’s modulus of bulk element, E [24]. It is suggested in the literature [36] that K should be set large enough to prevent the artificial compliance in cohesive element. Another concern of the cohesive zone method (CZM) implemented into FEM results from the length scale between the mesh size h_{mesh} and the cohesive zone length l_{cz}. The length of the cohesive zone imposes a constraint on the mesh size of the original bulk element. It has been reported in the literature that a minimum number of cohesive elements, e.g. 2 in [37] and more than 10 in [38], is needed in the cohesive zone to obtain reasonable FEM results.

However, the guidelines regarding the initial stiffness and mesh size in the literature are valid for cohesive elements only. As the combined interface model developed in the present study also involves the frictional contact mechanism, dedicated mesh convergence study needs to be performed and a suitable value for the initial stiffness should be specified. To this end, a representative shear test with a lateral confining pressure, a structural model inspired by the classical triplet experiment, was reproduced in our previous study. One can reference in [1,24] for the detailed numerical model set up and material properties for this investigation. The results show that the combined model requires a much finer mesh to get a convergence because of the involvement of contact-friction algorithm. However, a convergent result can be still obtained for both cohesion and friction when the mesh size is no larger than 5 mm for concrete-like materials. Regarding the initial stiffness, the results in [24] suggest that it generally has little influence on cohesion but has significant effect on friction response. In addition, it is dug out that this parameter can also control the activation time of the friction effect. A small value of initial stiffness introduces the friction effect from the very beginning of the shear process while a larger value triggers the friction only after a certain degree of 'separation'. In order to achieve a successful coupling such that both mechanisms can be enabled and a smooth transition from cohesion to pure friction can be realized, the suggest value for this parameter can be set as 50 times of the ratio of Young's modulus, E to the mesh size, h_{mesh}.

2.6 Model performance

The model shows good performance with no limitation of the friction coefficient (FC) or the normal compression on the interface. Figure 5 depicts the nominal shear stress against relative shear displacement with four representative frictional coefficients, namely, 0.3, 0.5, 0.7 and 0.9. The friction stress and the average cohesive stress against relative shear displacement for each friction coefficient are all presented in Figure 5(b) for reference. As shown, the model can also exhibit a continuous stable and smooth performance. A smooth transition from the decohesion process to the pure kinetic friction stage can be well captured for all the friction coefficients. As expected, the cohesion response is slighted influenced by the FC while the enhancement of the shear strength of the model mainly results from the friction effect.

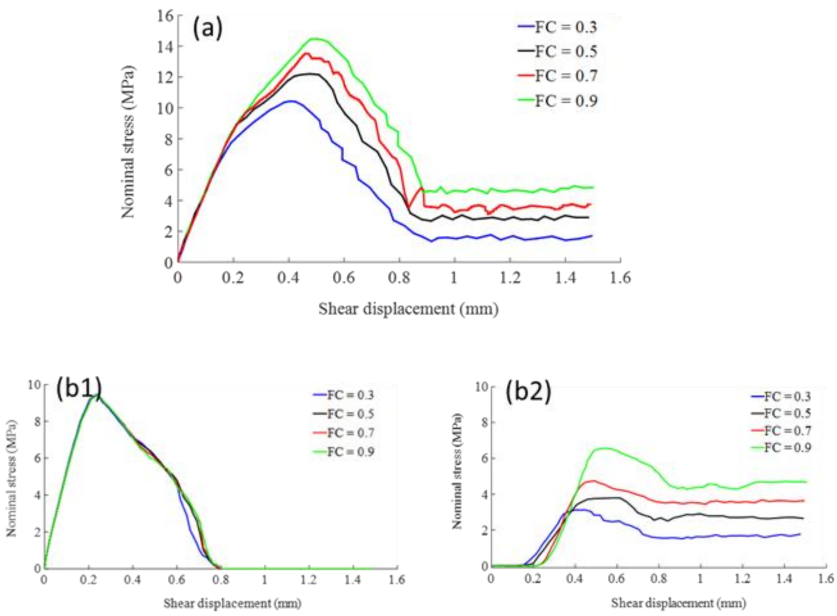

Figure 5 Model performance with different friction coefficient (FC): (a) Total shear stress vs. displacement; (b1) Cohesion stress; (b2) Friction stress.

Figure 6(a) presents the simulated shear stress vs. shear displacement curves for various levels of the normal compression pressures. It can be observed that the model successfully predicts a persistent increase in the shear strength as the normal compression increases. The separated evolutions of cohesion and friction from total shear stress under different normal pressures are shown in Figure 6(b). They confirm the model's capability in reproducing the residual shear stress which should be attributed to the basic friction effect (i.e. normal stress times the frictional coefficient).

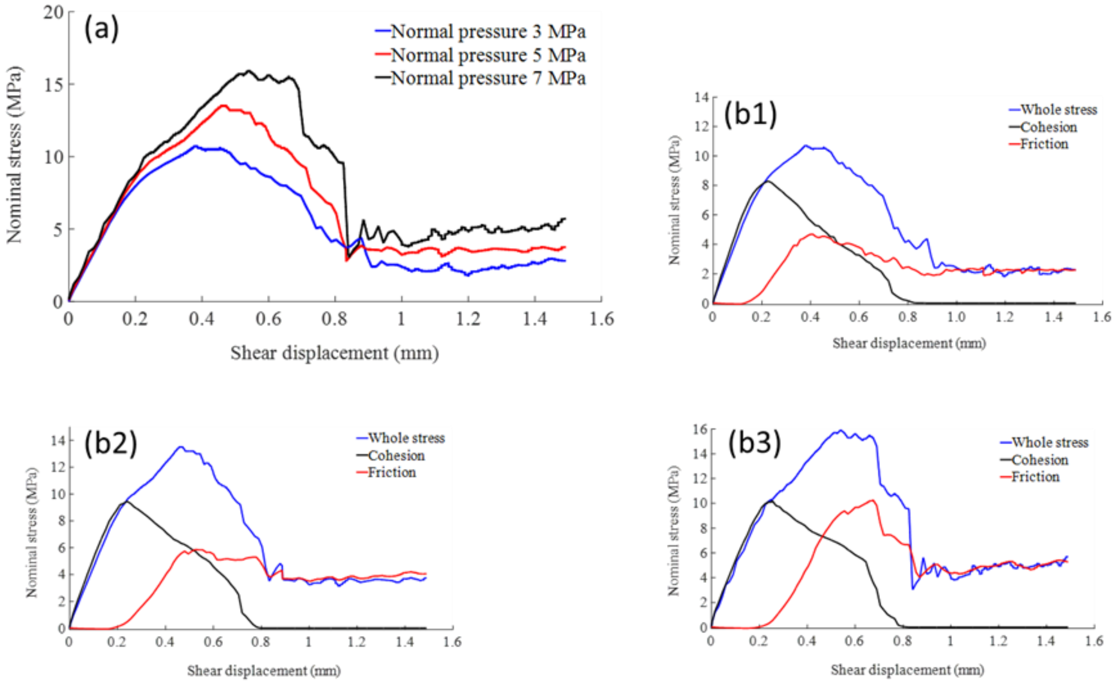

Figure 6 Model performance under different lateral pressures: (a) Total shear vs. shear displacement; (b) Evolution of the cohesion and friction with 3 MPa, 5 MPa and 7 MPa in (b1), (b2) and (b3) respectively.

The two examples presented above demonstrate the robustness of the proposed new model. This model is therefore deemed ready to be further applied in the mesoscale concrete framework to simulate the initiation and propagation of microcracks and the evolution of the FPZ in concrete. And this will be presented in the following sections.

3. Numerical simulation of evolution of fracture process zone in concrete

In this study, the experiment conducted by Wu et al. [39], in which the fracture process evolution of concrete was investigated based on three-point bending tests, is first chosen for the basic numerical model validation and verification. In the numerical model, the concrete in the critical region of the beams is modelled with the coupled mesoscale and cohesive-contact interface model described in Section 2. In this way, the evolution of the FPZ and the associated crack initiation, propagation and the friction mechanisms are comprehensively represented.

3.1 Model setup

The geometrical dimensions of the concrete beams and the loading method are set exactly the same as the ones used in the experimental tests [39]. Three concrete beams of different sizes, represented by a depth of $D = 40$, 60 and 80 mm, respectively, are modelled in the present study. For all the specimens, the span to height ratio was kept constant at $S/D = 4$ and the thickness also remained unchanged at $B = 40$ mm. The notch length to the section depth ratio is also kept constant at $a_0/D = 0.3$, as in the experiment. The details of the numerical model setup are shown in Figure 7.

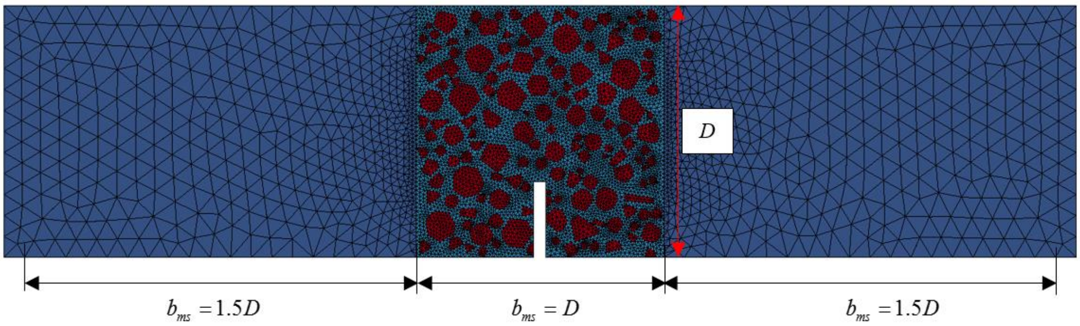

Figure 7 The numerical model set up

The observations from the experiment [39] and a previous numerical study [14] show that the damage zone only localizes in a region close to the notch while the remaining part of the beams is intact with no damage during the whole loading process. Therefore, in the present study, a ‘multi-scale’ approach is adopted, such that the meso-structure and cohesive contact interface element model is only used in the critical middle regions while the remaining parts of the beam are modelled as homogeneous materials with elastic properties resembling the average response of the concrete. Following the exploration in [14], the size of the mesoscale region is selected to be $b_{\mathrm{ms}} = D$ (see Figure 7).

3.2 Material parameters

Similar as the treatment in the triplet experiment in Section 2, the cracking procedure, as well as the softening behaviour of concrete is represented only via a constitutive relation between the traction and opening displacement in the cohesive elements. The bulk material outside the cohesive zone remains undamaged and it continues to behave linear-elastically. As mentioned in Section 2, a simple bilinear cohesive constitutive material model is adopted here, and this model considers the irreversible damage and allows for independent definitions of the constitutive relations for different fracture modes of tension and shear.

The material properties of the homogeneous parts of the beam model are directly taken from the experimental data but only the linear elastic response is considered, with Young's modulus being E = 35 GPa and the Poisson's ratio being v = 0.2. For the mesoscale model region in the middle part, the material properties for the different components are obtained such that the macro response of the concrete beam matches that in the experimental test, with consideration of the general considerations on the assignment of the material properties for a mesoscale concrete model as described in [24,32]. In the generation of the mesoscale geometry, only the coarse aggregates are considered to form the discrete aggregate phase. Smaller aggregates (< 2 mm in the present study) are lumped into the mortar phase. The volumetric ratio (or area ratio in 2D) of the coarse aggregates in the present study is in a range of 0.4–0.5 with the maximum aggregate size around 8 mm. The detailed properties for the bulk elements and the two interface components are given in Table 1 and Table 2 respectively. The properties used in the cohesive and contact interface elements, such as the initial stiffness K_N and K_S, the kinetic frictional coefficient μ are set according to our previous studies in [24]. The detailed values for these parameters are summarised in Table 3. It is worth noting that the ITZ interface properties are about 50% of the ones of the mortar matrix, which is in accordance with several published literature (e.g. [17,40]).

Table 1 Material properties for the bulk elements

Component	Density ρ (kg/mm^3)	Young's modulus E (MPa)	Poisson's ratio v (--)
Aggregate	2.6E3	7.0E4	0.2
Mortar	2.3E3	4.0E4	0.2

Table 2 Properties for the two interface components

Component	Tensile strength σ_I^P (MPa)	Fracture energy G_{IC} (N/mm)	Shear strength σ_{II}^P (MPa)	Fracture energy G_{IIC} (N/mm)

Mortar-mortar	4.7	0.06	18.8	0.6
Aggregate-mortar	2.3	0.03	9.2	0.3

Table 3 Properties for cohesive plus contact interface elements

Component	Normal stiffness K_N (MPa)	Shear stiffness K_S (MPa)	Frictional coefficient μ
Mortar-mortar	2.0E6	2.0E6	0.71
Aggregate-mortar	1.0E6	1.0E6	0.71

3.3 Mesh size effect

The mesoscopic cohesive plus contact interface model has already shown its advantage in obtaining a mesh independent result both globally and locally in relevant previous studies [24,32]. In view of these observations and the explicit representation of fracture in such a model, it is reasonable to consider that the evolution of the local fracture process can be well simulated in the current model in a rather mesh-independent manner, even no nonlocal approach for the bulk material description is employed. The simple shear test model given in Section 2, where similar material properties have been used, shows that a gross mesh grid size being h_{mesh}= 5 mm can yield a convergence result. For the mesoscale part of the beam model, the mesh size needs to be much finer than this to ensure the mesh convergence concerning the cohesive plus contact model. To confirm this, three different grid sizes, namely 2 mm, 1 mm, and 0.5 mm, are examined in the beam model with the smallest depth D = 40 mm. The corresponding results for both the global response and the local FPZ evolution are presented in Figure 8. The global response is represented by load vs. crack mouth opening displacement (CMOD) curves, in which the load is recorded as the force applied on the specimen while the CMOD is measured as the relative horizontal displacement of the points on the notch mouth shown in the figure.

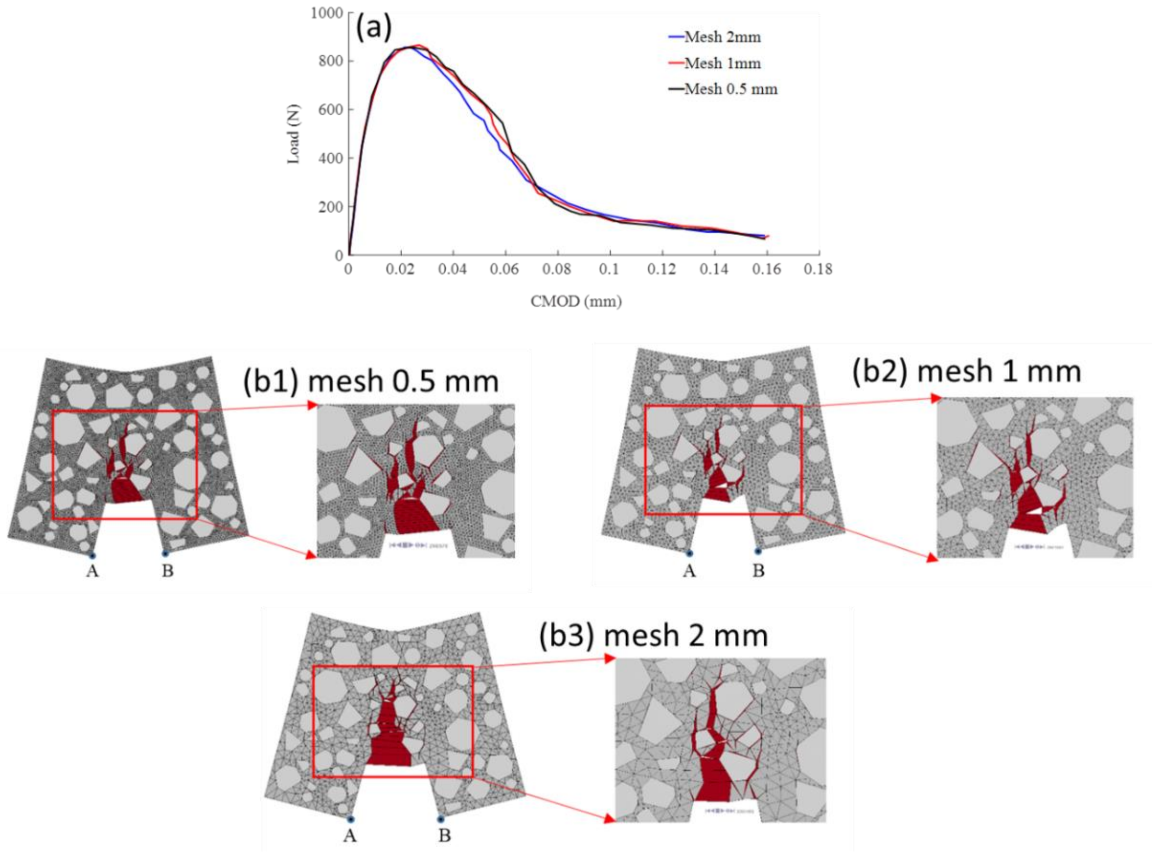

Figure 8 Mesh size studies: (a) global load-CMOD curves; (b) local crack patterns

As it is shown in Figure 8(a), the load vs. CMOD curve from the mesoscale cohesive plus contact model is indeed mesh-insensitive as expected. From the plots of the damage patterns shown in Figure 8(b), the FPZ widths obtained from the models with different meshes are almost identical. These observations clearly demonstrate the advantages of the current mesoscale model with a cohesive plus contact approach for the interfaces in obtaining a mesh independent result. It should be highlighted that these mesh independent results are obtained directly from the local fracture process without any other special treatment such as the fracture energy conservation or nonlocal approach which are generally used in a continuum-based numerical framework (e.g. [14]). Finally, a mesh size of 1 mm is adopted in the simulations presented in the remaining parts of this study.

3.4 Model verification

The numerical model is verified by comparing to the experiment results in [39], both globally by the load versus CMOD curve and locally by the evolution of the FPZ during the loading process.

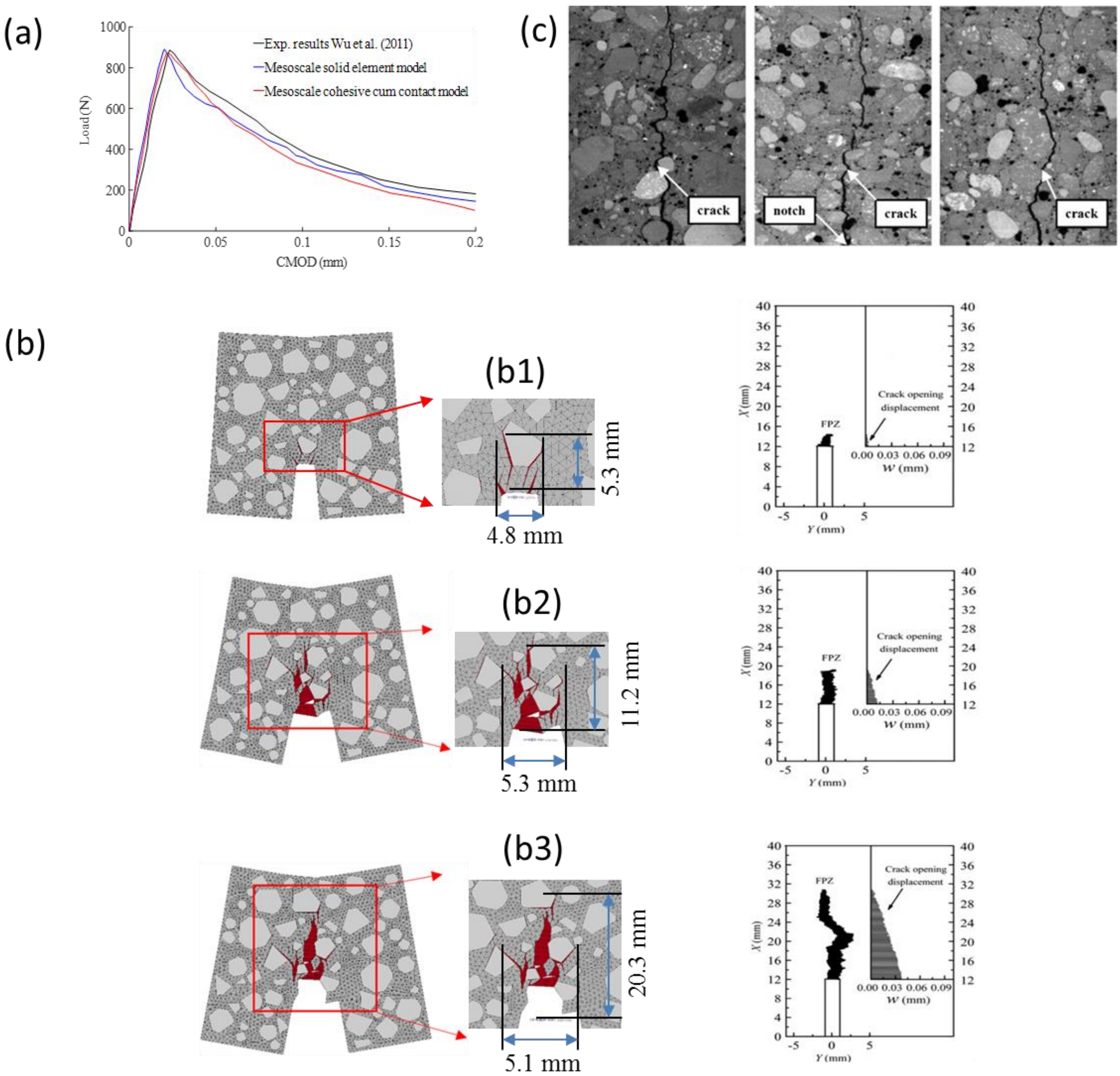

Figure 9 Model verification with experimental observation [39]: (a) load-CMOD curve; (b) crack patterns from three-point bending experiments [33](c) evolution of the FPZ with (b1) pre-peak, at 71.4% peak load, (b2) at peak load, and (b3) post-peak, at 60.6% peak load

Figure 9(a) shows a direct comparison of the load versus CMOD curve for the beam with D = 40 mm between numerical prediction and the experimental result. The corresponding development processes of the FPZ are further checked with experimental observations in Figure 9(b). Generally, both the length and width of the FPZ predicted from the present numerical model are larger than the ones from experimental measurements in [39]. At 71.4% pre-peak loading (Figure 9(b1)), the length of the FPZ from the numerical simulation is 4.8 mm, while the experimental measurement is around 2.4 mm. At peak loading (Figure 9(b2)), the length of the FPZ increases significantly to 11.2 and 7.2 mm for numerical prediction and experimental observation, respectively. At 60.6% post-peak loading, the length from the crack-tip to the notch is around 20.3 mm in numerical simulation and 19.6 mm in the numerical test. However, it can be clearly observed from the numerical model that the FPZ has already fully developed at this loading stage and a macrocrack is also formed above the notch. Therefore, the length of FPZ may be overestimated at this loading point. During all the loading process, the widths of the FPZ from both numerical simulation and experimental test are almost constant at 5 mm and 2 mm, respectively. The discrepancy on the size of the FPZ between numerical prediction and experimental observation may be interpreted as the difficulties in determining the small microcracks in experimental studies. Nevertheless, a very good agreement can still be observed for both the global response and the local fracture processes and this confirms that the current numerical model represents well the behaviour of the notched concrete beam.

Note that all the cracks in the present mesoscale fracture model are intergranular since the coarse aggregates are usually of much higher strength than the mortar matrix and nearly no damage can be found within them under quasi-static loading cases for normal concrete. This kind of intergranular crack is in good agreement with experimental observations (e.g. [33,34]).

4. Numerical simulation results and discussion

4.1 Evolution of FPZ

Figure 10-12 shows the evolution of the local fracture process in the three concrete beams from the current mesoscale model with cohesive plus contact interfaces. The fracture process is displayed directly from the deformation distributions, and in order to clearly observe the formation and evolution of the FPZ the deformation contours in all the models are scaled up by a factor of 200.

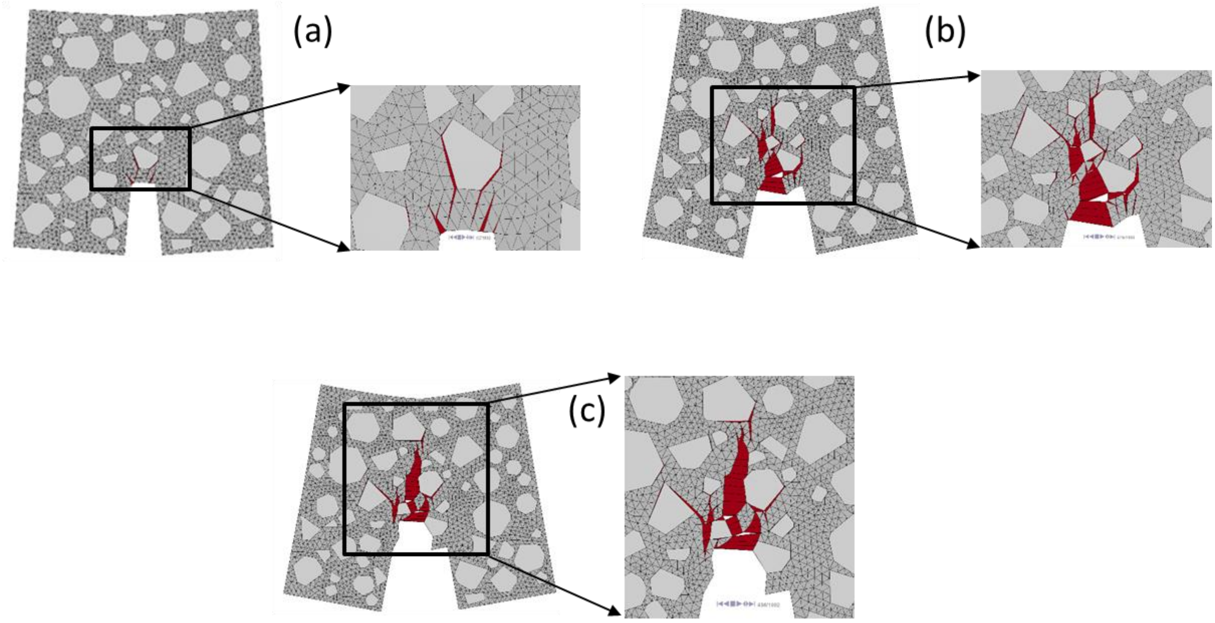

Figure 10 Evolution of the FPZ in the small concrete beam (D = 40 mm): (a) at a pre-peak stage (71.4% of the peak load); (b) around the peak load; (c) at a post-peak stage (60.6% of the peak load)

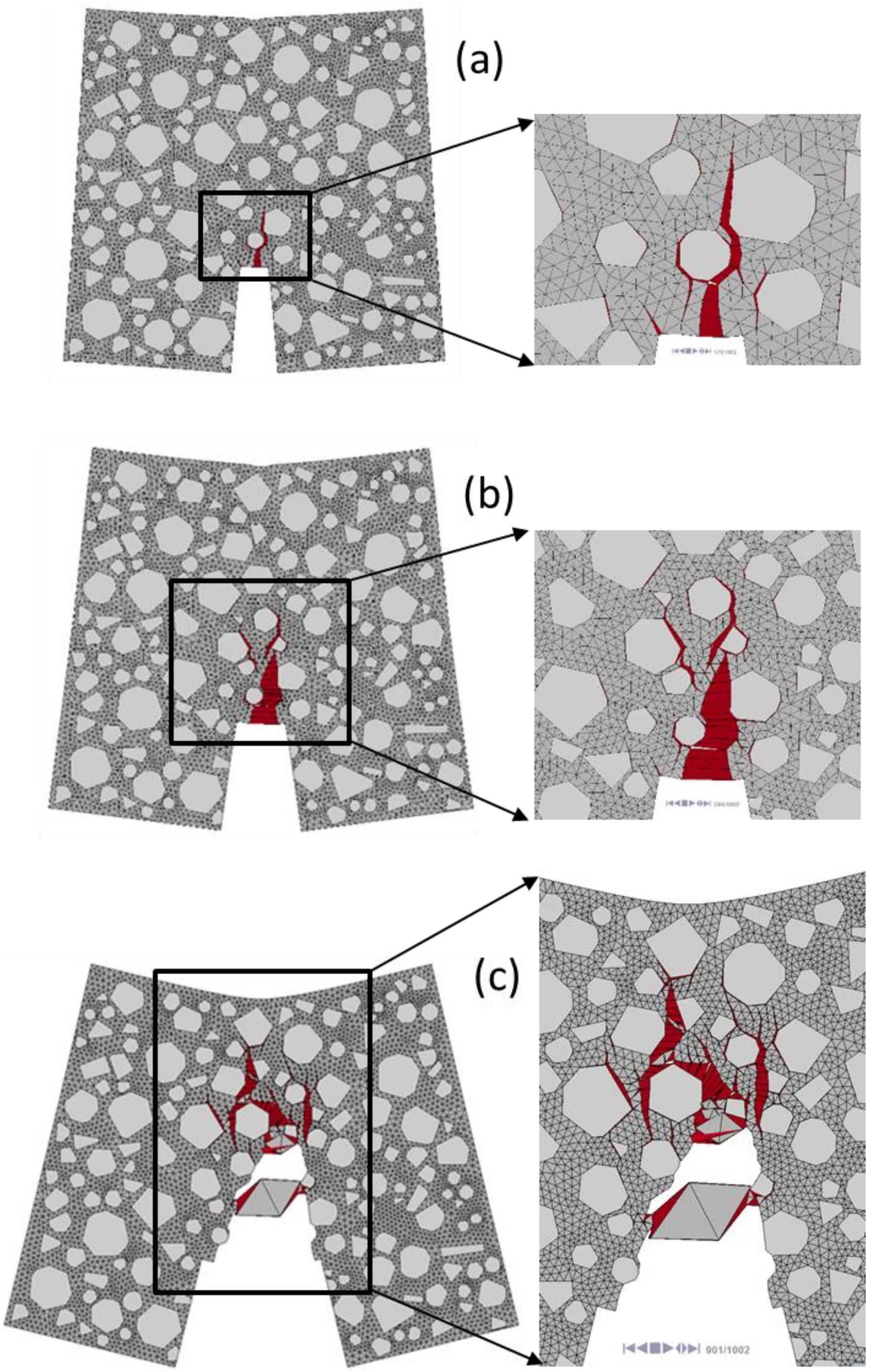

Figure 11 Evolution of the FPZ in the medium concrete beam (D = 60 mm): (a) at a pre-peak stage (85.1% of the peak load); (b) around the peak load; (c) at a post-peak stage (40% of peak load)

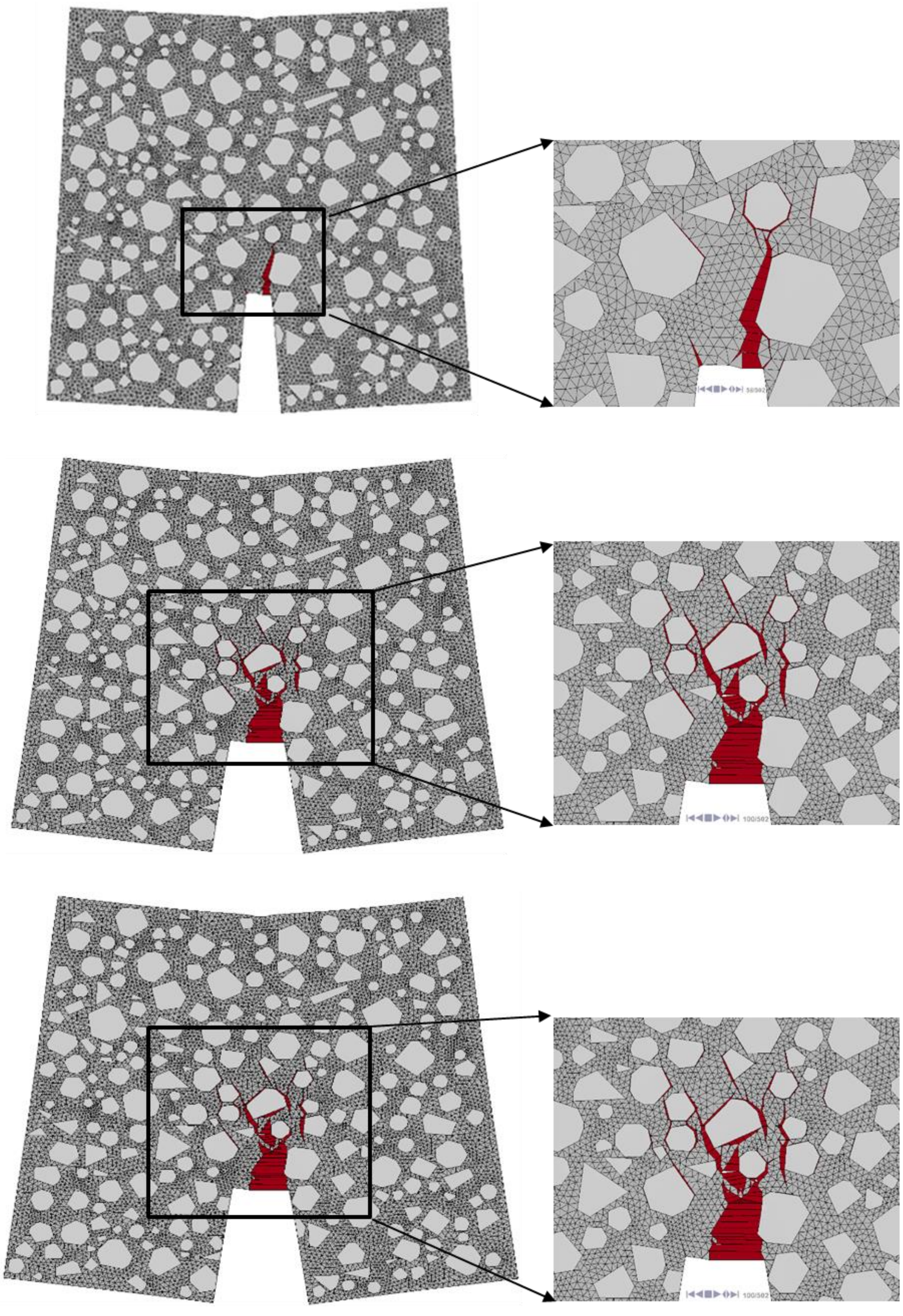

Figure 12 Evolution of the FPZ in the large concrete beam (D = 80 mm): (a) at a pre-peak stage (80.1% of the peak load); (b) around the peak load; (c) at a post-peak stage (31.4% of peak load).

As can be observed from Figure 10-12, the FPZ is actually composed with a main crack and many secondary microcracks. The main crack initiates above the notch due to the stress concentration at the notch tip. It then propagates upwards due to bending. The secondary microcracks mainly initiate and then propagate through the weak ITZs along the boundary of the strong aggregate particles. The main crack extends by bridging the interfacial micro-cracks which occur around adjacent aggregates. During the growth of the main crack, many new microcracks appear while some microcracks formed earlier stop growing and even close. The evolution path of the FPZ is strongly irregular due to the random spatial distribution of the aggregate particles with weak ITZs. Despite the strongly curved evolution path of the FPZ, the overall width of the FPZ remains almost constant throughout the fracture process for all the specimens.

The FPZ takes shape before the load reaches its maximum value and it can extend remarkably around the peak load. There is already a sizable FPZ at the peak load but the macro-crack has not formed yet. At the post-peak loading stage, the FPZ further extends upward with the appearance of many new microcracks. In the meantime, the macrocrack forms and propagates along the trajectory of the main crack in the FPZ. Since the extension of the FPZ is generally measured from the stress-free crack mouth ($\sigma_{\mathrm{traction}} = 0$) to the crack tip ($\sigma_{\mathrm{traction}} = \sigma_{\mathrm{peak}}$) [3,39], the length of the FPZ may gradually decrease during the post-peak stage.

The simulated process above regarding the development mechanism of cracks in concrete agree well with experimental observations based on DIC, X-ray and CT techniques (e.g. [41][42]). For a further examination, the shape and size of the FPZ at the peak load from the current cohesive and friction (CF) model and that using a continuum-based (CB) model are compared in Figure 13. To make a direct comparison, the two models use the same meso-structure and mesh size. In the CB model, the K&C concrete damage model (MAT_72R3 in LS-DYNA) with a non-local enhancement [43,44] is employed to describe the evolution of the FPZ.

From the comparison shown in Figure 13, the CF and CB models can be considered macroscopically equivalent as they predict similar results in terms of Load-CMOD curve. However, the development details of microcracks in the FPZ are not well captured and appear to be blurred in the continuum-based mesoscale model. On the other hand, the current mesoscale model with cohesive plus contact interfaces is clearly advantageous in capturing the very local fracture process in concrete materials.

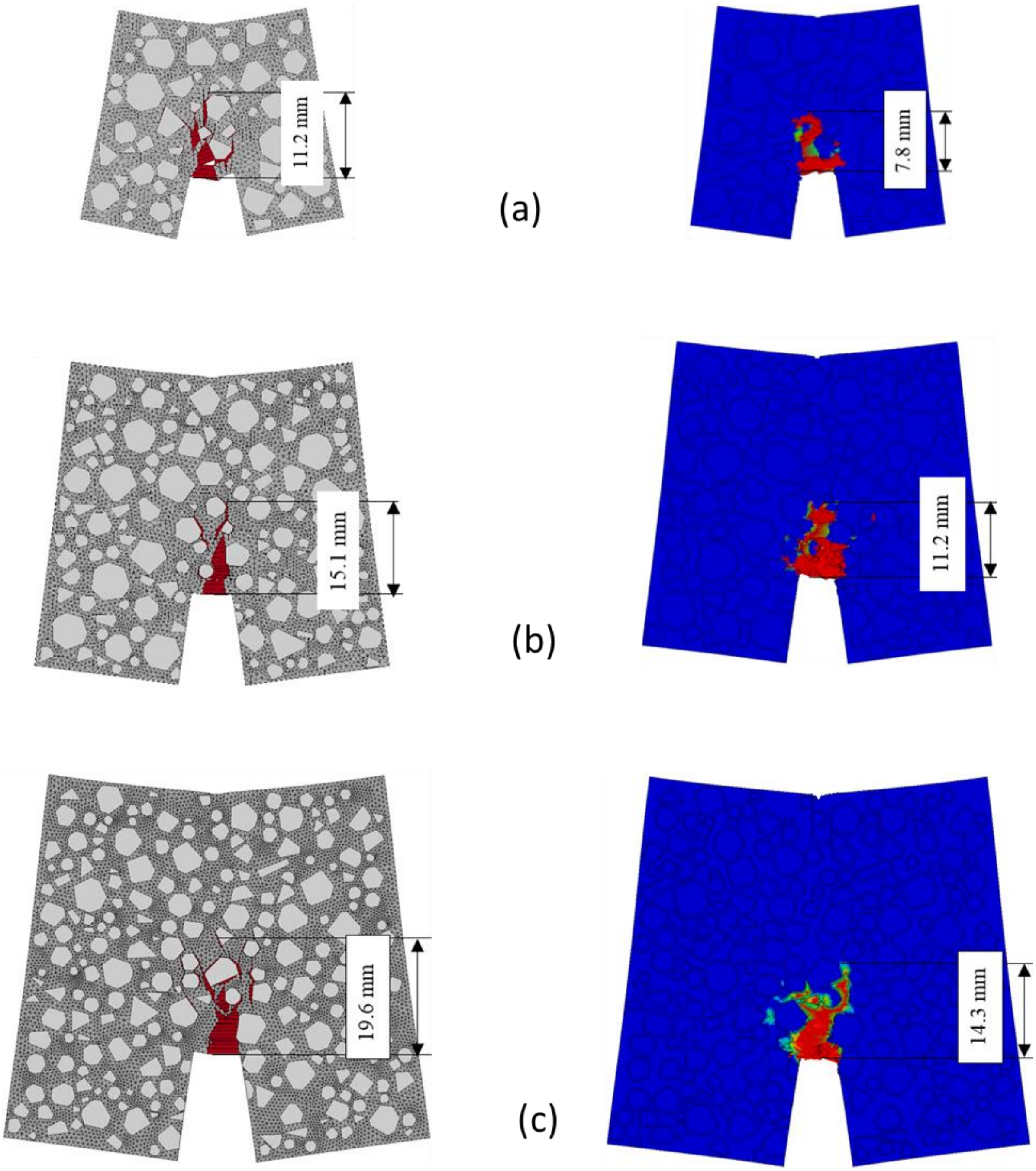

Figure 13 Comparison between cohesive plus friction model and the continuum-based model (left: cohesive plus contact model, right: continuum-based model): (a) small beam D = 40 mm; (b) medium beam D = 60 mm; (c) large size D = 80 mm

From the details of fracture produced by the mesoscale with cohesive plus contact interface model, it can be found that the main crack is generally in a mode-I fracture mode, but mode-II and mixed-mode fracture are present in several microcracks within the FPZ. This reveals the complex local stress condition and fracture process that are closely related to the random distribution of the aggregate particles. It further confirms that a comprehensive numerical modelling framework capable of incorporating the meso-structure and the evolving shear and normal traction as well as the friction effects is necessary in order to realistically track the evolution of the FPZ in concrete. The present model serves well this purpose.

4.2 Size effect on the FPZ

As stated earlier, the FPZ is very important in determining the macro fracture and failure behaviour of concrete materials. However, due to the complexity of the internal structure of the concrete materials, a very basic question remains as whether the size of the FPZ is dependent upon the specimen size or it can be considered as an intrinsic material property. To provide insight into this subject from the current mesoscale and cohesive-contact description point of view, an extended number of five beams are simulated. These beams all have the same geometry, but different sizes including D = 40, 60, 80, 120 and 160 mm, respectively.

Figure 14 shows the shapes and sizes of the FPZ at peak loading point for the five specimens. As can be observed, the absolute widths of the FPZ are almost the same (around 5 mm) for all the specimens. This phenomenon is consistent with the observations reported by Skarżyński et al.[44] using the DIC technique and previous numerical work by Grassl et al.[12]. It suggests that the width of the FPZ may be considered as a material property. As a matter of fact, in the crack band theory, the width of the FPZ is already assumed to be a constant and a typical value is given as three times of maximum aggregate size [45]. The results in the present simulations clearly indicate that the width of the FPZ is indeed dependent on the sizes of the aggregates along the crack propagation path, but it appears to be smaller than the assumed value above.

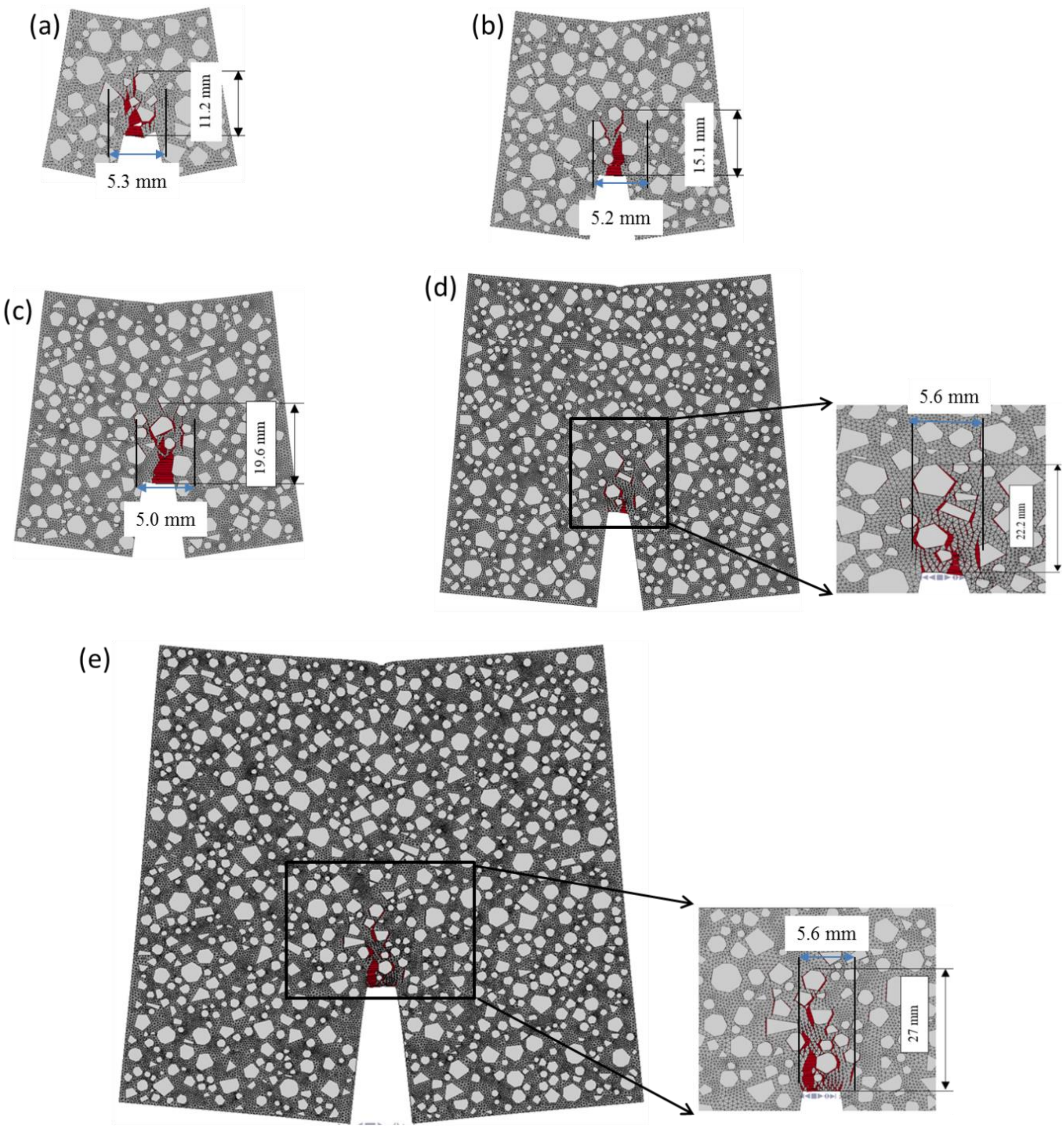

Figure 14 The shape and size of the FPZ for different sized beams: (a) D = 40 mm; (b) D = 60 mm; (c) D = 80 mm; (d) D = 120 mm; (e) D = 160 mm

On the other hand, the absolute length of the FPZ at the peak loading point appears to be strongly dependent on the specimen size. As can be clearly seen, the greater the specimen size, the longer the FPZ. The length increases from around 11.2 mm for the smallest beam ($D = 40$ mm) to 27 mm for the largest beam (D = 160 mm). This strong dependence of the fracture zone length on the size may be explained by the decrease of stress gradient with the increase of the beam size. However, in terms of the relative or normalised FPZ length, i.e. the ratio of the length of the FPZ to the ligament length above the notch, l_{FPZ}/H at the peak load, an opposite trend can be observed, such that the ratio decreases as the specimen size increases. The trend is plotted in Figure 15. This result from the current numerical simulation actually echoes nicely the observations made from experimental studies [39,43]. In addition, comparison between the CF and CB models show that the cohesive plus contact model predicts much longer length of the FPZs than the continuum-based model does. Despite similar tendency, the continuum model fails to capture the rate of decrease of the normalised FPZ length with increase the specimen size. Nevertheless, it is reasonable to state that the length of the FPZ, whether in absolute or normalised term, is not a material parameter but is dependent on the specimen size.

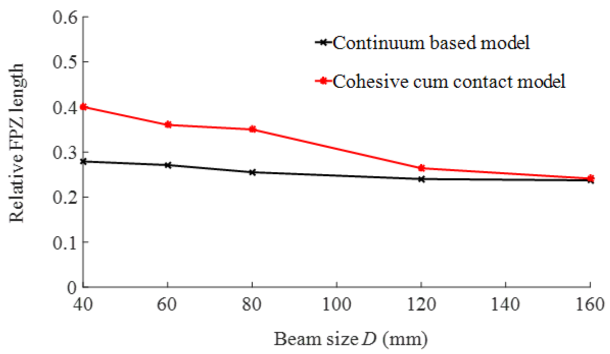

Figure 15 Comparison of the relative FPZ length at peak load

5. Conclusions

The present study proposes to use a coupled cohesive and friction interface model to simulate the crack initiation, crack propagation and the friction mechanisms during the fracture process in concrete materials and study the characteristics of the fracture process zone (FPZ). The performance of coupled cohesive and contact-friction interface approach is first verified in a triplet shear configuration with varying lateral pressure. The model is then implemented into a mesoscale concrete framework for investigating the evolution of FPZ, using notched plain concrete beams subjected to three-point bending.

The numerical modelling results have brought new insights into the mechanisms of evolution of the FPZ from the perspective of micro-crack initiation and propagation. With the details of main and secondary fractures being explicitly captured, the width of the FPZ is found to remain almost constant during the process of fracture; and furthermore, it is insensitive to the size of the concrete beams. This indicates that the width of the FPZ may indeed be considered as a material parameter. On the contrary, the length of the FPZ shows continued increase with the loading, and it is strongly dependent on the specimen size. The absolute FPZ length at the peak loading point increases significantly with the increase of the specimen size. However, when normalised with respect to the ligament length above the notch, the normalised FPZ length shows an opposite tendency. These characteristics in the width and length of the FPZ would underpin the widely recognised size effect phenomenon in concrete materials.

The comparative results also suggest that there is marked limitation with the continuum-based model in terms of the ability to capture the mechanisms of the micro-crack initiation and propagation in the concrete.

This study paves a way for further application of the mesoscale cohesive plus friction model to investigate the evolution of the FPZ under mixed fracture mode loadings, e.g., mixed mode-I and mode-II crack propagation in concrete, where the effect of the friction mechanisms on the evolution of the FPZ is anticipated to play a more significant role.

References

[1] Zhou R, Rongxin. Mesoscopic analysis of damage mechanisms in concrete material. The University of Edinburgh, 2016. doi:https://www.era.lib.ed.ac.uk/handle/1842/23650.

[2] Doll B, Ozer H, Rivera-Perez J, Al-Qadi IL, Lambros J. Damage zone development in heterogeneous asphalt concrete. Eng Fract Mech 2017;182:356–71. doi:10.1016/J.ENGFRACMECH.2017.06.002.

[3] Dong W, Wu Z, Zhou X, Wang N, Kastiukas G. An experimental study on crack propagation at rock-concrete interface using digital image correlation technique. Eng Fract Mech 2017;171:50–63. doi:10.1016/J.ENGFRACMECH.2016.12.003.

[4] Li L, Sun S, Wang J, Yang W, Song S, Fang Z. Experimental study of the precursor information of the water inrush in shield tunnels due to the proximity of a water-filled cave. Int J Rock Mech Min Sci 2020;130:104320. doi:10.1016/J.IJRMMS.2020.104320.

[5] Hu X, Duan K, Hu X, Duan K. Size effect and quasi-brittle fracture: the role of FPZ. Int J Fract 2008;154:3–14. doi:10.1007/s10704-008-9290-7.

[6] Saliba J, Matallah M, Loukili A, Regoin JP, Grégoire D, Verdon L, et al. Experimental

and numerical analysis of crack evolution in concrete through acoustic emission technique and mesoscale modelling. Eng Fract Mech 2016;167:123–37. doi:10.1016/J.ENGFRACMECH.2016.03.044.
[7] Swartz SE. Dye Techniques To Reveal the Fracture Surface of Concrete in Mode I. Exp Tech 1991;15:29–34. doi:10.1111/j.1747-1567.1991.tb01177.x.
[8] Hadjab-Souag H, Thimus J-FF, Chabaat M. Detecting the fracture process zone in concrete using scanning electron microscopy and numerical modelling using the nonlocal isotropic damage model. vol. 34. NRC Research Press Ottawa, Canada ; 2007.
[9] Ohno K, Uji K, Ueno A, Ohtsu M. Fracture process zone in notched concrete beam under three-point bending by acoustic emission. Constr Build Mater 2014;67:139–45.
[10] Li S, Fan X, Chen X, Liu S, Guo Y. Development of fracture process zone in full-graded dam concrete under three-point bending by DIC and acoustic emission. Eng Fract Mech 2020;230:106972. doi:10.1016/j.engfracmech.2020.106972.
[11] Fakhimi A, Tarokh A. Process zone and size effect in fracture testing of rock. Int J Rock Mech Min Sci 2013;60:95–102. doi:10.1016/J.IJRMMS.2012.12.044.
[12] Grassl P, Grégoire D, Rojas Solano L, Pijaudier-Cabot G. Meso-scale modelling of the size effect on the fracture process zone of concrete. Int J Solids Struct 2012;49:1818–27. doi:10.1016/J.IJSOLSTR.2012.03.023.
[13] Skarżyński Ł, Tejchman J. Experimental Investigations of Fracture Process Using DIC in Plain and Reinforced Concrete Beams under Bending. Strain 2013;49:521–43. doi:10.1111/str.12064.
[14] Zhou R, Chen H-M. Mesoscopic investigation of size effect in notched concrete beams: The role of fracture process zone. Eng Fract Mech 2019;212:136–52. doi:10.1016/J.ENGFRACMECH.2019.03.028.
[15] Eliáš J, Vořechovský M. Fracture in random quasibrittle media: I. Discrete mesoscale simulations of load capacity and fracture process zone. Eng Fract Mech 2020;235:107160. doi:10.1016/j.engfracmech.2020.107160.
[16] Vořechovský M, Eliáš J. Fracture in random quasibrittle media: II. Analytical model based on extremes of the averaging process. Eng Fract Mech 2020;235:107155. doi:10.1016/j.engfracmech.2020.107155.
[17] Zhou R, Song Z, Lu Y. 3D mesoscale finite element modelling of concrete. Comput Struct 2017;192:96–113. doi:10.1016/J.COMPSTRUC.2017.07.009.
[18] Lu Y. Modelling the dynamic response of concrete with mesoscopic heterogeneity.

2013. doi:10.1533/9780857097538.2.218.

[19] Grassl P, Jirásek M. Meso-scale approach to modelling the fracture process zone of concrete subjected to uniaxial tension. Int J Solids Struct 2010;47:957–68. doi:10.1016/j.ijsolstr.2009.12.010.

[20] Nitka M, Tejchman J. Meso-mechanical modelling of damage in concrete using discrete element method with porous ITZs of defined width around aggregates. Eng Fract Mech 2020;231:107029. doi:10.1016/j.engfracmech.2020.107029.

[21] Nitka M, Tejchman J. A three-dimensional meso-scale approach to concrete fracture based on combined DEM with X-ray μCT images. Cem Concr Res 2018;107:11–29. doi:10.1016/j.cemconres.2018.02.006.

[22] Thilakarathna PSM, Kristombu Baduge KS, Mendis P, Chandrathilaka ERK, Vimonsatit V, Lee H. Understanding fracture mechanism and behaviour of ultra-high strength concrete using mesoscale modelling. Eng Fract Mech 2020;234:107080. doi:10.1016/j.engfracmech.2020.107080.

[23] Thilakarathna PSM, Kristombu Baduge KS, Mendis P, Vimonsatit V, Lee H. Mesoscale modelling of concrete – A review of geometry generation, placing algorithms, constitutive relations and applications. Eng Fract Mech 2020;231:106974. doi:10.1016/j.engfracmech.2020.106974.

[24] Zhou R, Lu Y. A mesoscale interface approach to modelling fractures in concrete for material investigation. Constr Build Mater 2018;165:608–20. doi:10.1016/J.CONBUILDMAT.2018.01.040.

[25] Skarżyński Ł, Tejchman J. Calculations of fracture process zones on meso-scale in notched concrete beams subjected to three-point bending. Eur J Mech - A/Solids 2010;29:746–60. doi:10.1016/J.EUROMECHSOL.2010.02.008.

[26] Dong W, Wu Z, Zhou X, Dong L, Kastiukas G. FPZ evolution of mixed mode fracture in concrete: Experimental and numerical. Eng Fail Anal 2017;75:54–70. doi:10.1016/J.ENGFAILANAL.2017.01.017.

[27] Wang J, Jivkov AP, Li QM, Engelberg DL. Experimental and numerical investigation of mortar and ITZ parameters in meso-scale models of concrete. Theor Appl Fract Mech 2020;109:102722. doi:10.1016/j.tafmec.2020.102722.

[28] Lu Y, Zhou R. Holistic mesoscale modelling of concrete – Recent developments. Proc. 14th Int. Conf. Comput. Plast. - Fundam. Appl. COMPLAS 2017, vol. 2017- Janua, 2017.

[29] Lu Y, Zhou R. Holistic mesoscale modelling of concrete-recent developments. n.d.
[30] Trawiński W, Tejchman J, Bobiński J. A three-dimensional meso-scale modelling of concrete fracture, based on cohesive elements and X-ray μCT images. Eng Fract Mech 2018;189:27–50. doi:10.1016/J.ENGFRACMECH.2017.10.003.
[31] Tu Z, Lu Y. Mesoscale modelling of concrete for static and dynamic response analysis -Part 1: model development and implementation. Struct Eng Mech 2011;37:197–213. doi:10.12989/sem.2011.37.2.197.
[32] Zhou R, Chen H-M, Lu Y. Mesoscale modelling of concrete under high strain rate tension with a rate-dependent cohesive interface approach. Int J Impact Eng 2020:103500. doi:10.1016/J.IJIMPENG.2020.103500.
[33] Skarzyński, Nitka M, Tejchman J. Modelling of concrete fracture at aggregate level using FEM and DEM based on X-ray μCT images of internal structure. Eng Fract Mech 2015;147:13–35. doi:10.1016/j.engfracmech.2015.08.010.
[34] Du Plessis A, Boshoff WP. A review of X-ray computed tomography of concrete and asphalt construction materials. Constr Build Mater 2019;199:637–51. doi:10.1016/j.conbuildmat.2018.12.049.
[35] Gerlach S, Fiolka M. Modelling and analysis of adhesively bonded joints with interface elements for crash analysis. LS- 2005:35–44.
[36] Turon A, Dávila CGG, Camanho PPP, Costa J. An engineering solution for mesh size effects in the simulation of delamination using cohesive zone models. Eng Fract Mech 2007;74:1665–82. doi:10.1016/j.engfracmech.2006.08.025.
[37] Falk ML, Needleman A, Rice JR. A critical evaluation of cohesive zone models of dynamic fracture. J. Phys. IV JP, vol. 11, 2001. doi:10.1051/jp4:2001506.
[38] Moës N, Belytschko T. Extended finite element method for cohesive crack growth. Eng Fract Mech 2002;69:813–33. doi:10.1016/S0013-7944(01)00128-X.
[39] Wu Z, Rong H, Zheng J, Xu F, Dong W. An experimental investigation on the FPZ properties in concrete using digital image correlation technique. Eng Fract Mech 2011;78:2978–90. doi:10.1016/J.ENGFRACMECH.2011.08.016.
[40] Yılmaz O, Molinari J-F. A mesoscale fracture model for concrete. Cem Concr Res 2017;97:84–94. doi:10.1016/J.CEMCONRES.2017.03.014.
[41] Bhowmik S, Ray S. An experimental approach for characterization of fracture process zone in concrete. Eng Fract Mech 2019;211:401–19. doi:10.1016/J.ENGFRACMECH.2019.02.026.

[42] Skarżyński Ł, Tejchman J. Experimental investigations of damage evolution in concrete during bending by continuous micro-CT scanning. Mater Charact 2019;154:40–52. doi:10.1016/J.MATCHAR.2019.05.034.

[43] Alam SY, Kotronis P, Loukili A. Crack propagation and size effect in concrete using a non-local damage model. Eng Fract Mech 2013;109:246–61. doi:10.1016/J.ENGFRACMECH.2013.07.009.

[44] Skarżyński Ł, Syroka E, Tejchman J. Measurements and Calculations of the Width of the Fracture Process Zones on the Surface of Notched Concrete Beams. Strain 2011;47:e319–32. doi:10.1111/j.1475-1305.2008.00605.x.

[45] Bažant ZP, Oh BH. Crack band theory for fracture of concrete. Matériaux Constr 1983;16:155–77. doi:10.1007/BF02486267.